

New precise half-life measurement for the superallowed β^+ emitter ^{34}Ar

V. E. Iacob,^{*} J. C. Hardy,[†] H. I. Park, M. Bencomo, L. Chen, V. Horvat, N. Nica, B. T. Roeder, and A. Saastamoinen
Cyclotron Institute, Texas A&M University, College Station, Texas 77843-3366, USA

 (Received 13 November 2019; published 21 January 2020)

We have measured the half-life of ^{34}Ar , the parent of a superallowed $0^+ \rightarrow 0^+$ β transition, to be 0.84646(35) s. With a precision of 0.04%, this result is an essential ingredient needed to complete a third pair of mirror superallowed transitions, $^{34}\text{Ar} \rightarrow ^{34}\text{Cl}$ and $^{34}\text{Cl} \rightarrow ^{34}\text{S}$, the ratio of whose ft values would provide the most sensitive test yet of the isospin-symmetry-breaking corrections used to obtain V_{ud} . In a sequence repeated thousands of times, we implanted a very pure ^{34}Ar beam into tape for 0.7 s, and then rapidly transported the collected source to a shielded 4π proportional gas counter, which detected the decay positrons from the combined decays of ^{34}Ar and its daughter ^{34}Cl . The data were analyzed as a linked parent-daughter pair. Our new result replaces one we published 13 years ago.

DOI: [10.1103/PhysRevC.101.015504](https://doi.org/10.1103/PhysRevC.101.015504)

I. INTRODUCTION

Currently, superallowed $0^+ \rightarrow 0^+$ β decay provides the most precise value for V_{ud} , the up-down element of the Cabibbo-Kobayashi-Maskawa (CKM) quark-mixing matrix, and makes possible the most demanding test of that matrix's unitarity. The latest critical survey of world data on superallowed transitions [1] included 14 transitions known well enough to contribute to the extraction of V_{ud} . Of those 14, the ft value for the transition from ^{34}Ar was the *least* precisely known, even though its relative uncertainty was a respectable $\pm 0.27\%$.

Improving the precision of the ^{34}Ar result would be of marginal significance if it were not for the fact that this superallowed transition has become a particularly interesting case. It is one of the few accessible superallowed transitions to have a mirror-decay partner, in this case $^{34}\text{Cl} \rightarrow ^{34}\text{S}$. We have previously reported on two other mirror pairs, $^{38}\text{Ca} \rightarrow ^{38m}\text{K} \rightarrow ^{38}\text{Ar}$ [2] and $^{26}\text{Si} \rightarrow ^{26m}\text{Al} \rightarrow ^{26}\text{Mg}$ [3], after pointing out [4] that a high-precision comparison of the ft values from a pair of mirror superallowed transitions provides a very sensitive test of the isospin-symmetry-breaking correction needed to extract V_{ud} from the experimental ft values. The $A = 34$ mirror pair has the potential to yield a more precise mirror-pair comparison, and so a more sensitive test, than either of the two other pairs.

The reason is best explained with reference to the decay scheme illustrated in Fig. 1, where it can be seen that the intensities of the Gamow-Teller decay branches from ^{34}Ar sum to less than 6% of the total decay intensity, leaving the superallowed branch to carry the remaining $\approx 94\%$. Since it is the former intensity that is actually measured and then subtracted from 100% to obtain the latter, the relative precision obtained

in the measured Gamow-Teller intensity is improved by a factor of ≈ 17 when it is applied to the superallowed branch. Since the only measurement of this branching ratio was made 45 years ago [8], there is a good opportunity for improvement with modern techniques, and such a measurement by our group is well advanced. At the same time, it is also important that the half-life be established with equivalent precision and accuracy. That is the purpose of the measurement reported here.

The weakness of the Gamow-Teller branches from ^{34}Ar , which offers the advantage just described for a

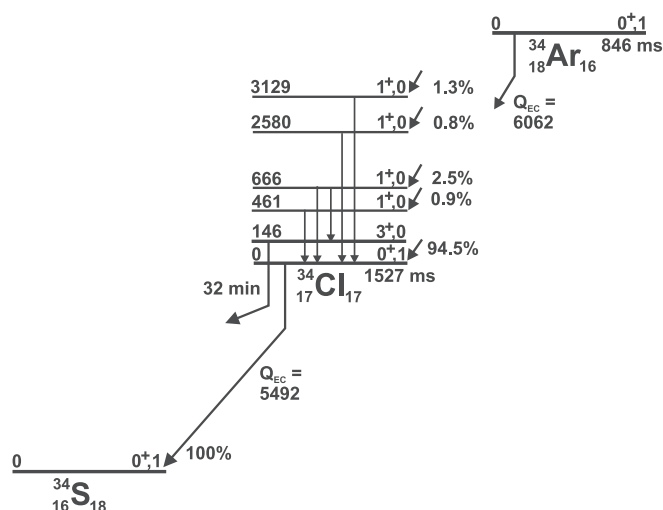


FIG. 1. Beta-decay schemes of ^{34}Ar and ^{34}Cl , showing the mirror superallowed transitions and those other features relevant to the half-life measurement reported here. Each level in ^{34}Cl is labeled with its (J^π, T) as well as its excitation energy, expressed in keV. Basic content is from the 2012 evaluation [5]; however, the branching percentages and the presence of a 519-keV γ -ray transition between the 666- and 146-keV levels come from more recent measurements [6,7].

^{*}iacob@comp.tamu.edu

[†]hardy@comp.tamu.edu

branching-ratio determination, has the opposite effect on any half-life measurement that depends on the detection of β -delayed γ rays. Since ^{34}Ar decays by positron emission, more than 97% of the photons arising from its decay are due to annihilation radiation. Dead-time considerations limit the total acceptable counting rate for detected photons, which leaves the rate of the 666-keV photons of interest much too low for adequate statistics to be acquired in a realistic amount of accelerator beam time.

Our approach is to detect the positrons directly. This has the advantage of high efficiency and low dead time, but it also has the disadvantage that the decays of both ^{34}Ar and its daughter ^{34}Cl are detected together and must be disentangled in analysis. As described in the following sections, we employ a number of specialized features in data acquisition and in analysis that make this possible.

Our first measurement of this type was also of the ^{34}Ar half-life; it was published in 2006 [9]. At that time many of the specialized features had not yet been optimally employed, although we only recognized the impact of these deficiencies quite recently. Before subsequent half-life measurements were made of other similar cases [10–12] we had rectified the deficiencies and optimally applied all the features that we use here to revisit the ^{34}Ar half-life. We offer the new result as a replacement for our earlier one [9], which we withdraw.

II. EXPERIMENT

A. Overview

We produced 0.85-s ^{34}Ar via the $p(^{35}\text{Cl}, 2n)^{34}\text{Ar}$ reaction initiated by a 30A-MeV ^{35}Cl beam from the K500 superconducting cyclotron at Texas A&M University. The target was liquid-nitrogen-cooled hydrogen gas contained at 2.0 atm pressure in a thin-walled gas cell located within the target chamber of the Momentum Achromat Recoil Spectrometer (MARS) [13]. The fully stripped reaction products recoiled into MARS, where they were spatially separated according to their charge-to-mass ratio, q/m , leaving a 99.5% pure ^{34}Ar beam to emerge from the focal-plane acceptance slits. This beam exited the vacuum system through a 51- μm -thick Kapton window, passed through a 0.3-mm-thick BC-404 scintillator and a stack of aluminum degraders, before finally stopping in the 76- μm -thick aluminized Mylar tape of a fast tape-transport system.

After ^{34}Ar had been collected in the tape for 0.7 s, the cyclotron beam was turned off and the tape-transport system moved the collected sample rapidly to a well-shielded location 90 cm away, where it halted at the center of a 4π proportional gas counter. Decay positrons were then recorded, starting 210 ms after the beam had been turned off and continuing for 16.2 s, equivalent to just over 19 half-lives of ^{34}Ar . With counting complete, the cyclotron beam was turned on again and the cycle was repeated. The timing of these collect-move-detect cycles was controlled by the tape-transport system's precision clock, and was continuously monitored by our data-acquisition system. The cycles were repeated until the desired statistics had been achieved. For this measurement, we collected data from nearly 12 000 cycles divided into

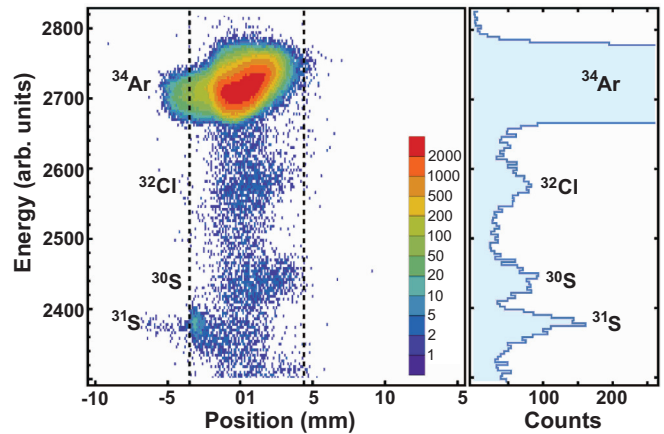


FIG. 2. The deposited energy versus position as obtained with the PSSD in the MARS focal plane. The spectrometer had already been optimized for ^{34}Ar production and the acceptance slits (vertical dotted lines) had been set 7.5 mm apart. On the right is a projection on the energy axis. Spectra were acquired every 24 hours, with the figure showing the sum of several. We established that the total contribution of ^{32}Cl , ^{30}S , and ^{31}S to the extracted ^{34}Ar beam was 0.32(6)%.

36 separate runs, which yielded a total of 1.7×10^8 beta counts.

B. Source purity

After the primary ^{35}Cl beam from the cyclotron had been fully tuned, we optimized the secondary ^{34}Ar beam purity through MARS before the measurement began. First, we inserted an attenuating grid into the cyclotron injection line to reduce the primary beam intensity, allowing us to place a 1-mm-thick 16-strip position-sensitive silicon detector (PSSD) at the MARS focal plane. Then, with the low-current primary beam, we focused the ^{34}Ar beam, identified nearby reaction products and minimized those that could affect the purity of the beam. Once spectrometer tuning had been completed, we set the focal-plane acceptance slits 7.5 mm apart and recorded the result shown in Fig. 2. In addition to ^{34}Ar , the figure shows the weak presence of three residual impurities: ^{32}Cl ($T_{1/2} = 298$ ms), ^{30}S ($T_{1/2} = 1.18$ s), and ^{31}S ($T_{1/2} = 2.55$ s). Their respective intensities are 0.10(1)%, 0.09(1)%, and 0.13(2)% relative to that of ^{34}Ar . There are also some weak lighter-mass impurities cut off from the figure but they all have a much longer range than the ^{34}Ar ions and pass entirely through the collection tape. None of these play any role in the measurement.

Following the tuning of MARS, the PSSD was removed from the beam path and the attenuating grid was withdrawn from the injection line, restoring the full primary beam intensity without any change in cyclotron or beam-line parameters. Data collection then began. Subsequently, once per day we checked the composition of the extracted beam by reinserting the attenuating grid and the PSSD, and acquiring a spectrum equivalent to the one shown in Fig. 2. On several occasions, some increase in impurity intensity was observed, which was then corrected by small adjustments to the MARS

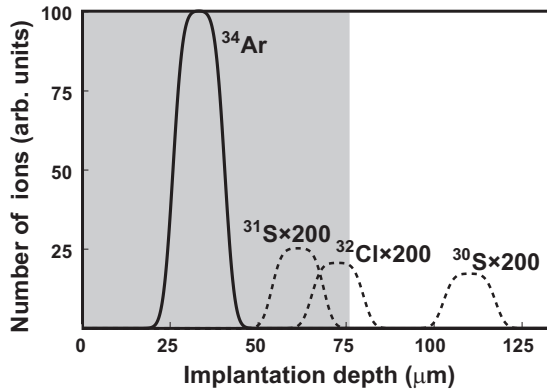


FIG. 3. Implantation profiles of ^{34}Ar (solid line) and the three contaminant activities ^{31}S , ^{32}Cl , and ^{30}S (dashed lines). The beam enters from the left. The shaded region shows the actual thickness of the Mylar collection tape. Our collected source contains only those ions that are stopped in the tape.

tuning parameters. The potential impact of these temporary increases is reflected in the uncertainties we quote on the impurity percentages.

Of course, the composition of the extracted radioactive beam that is revealed in Fig. 2 is not exactly the same as the composition of the sample deposited in the collection tape. The components of the beam are affected differently by the degraders located in front of the tape.

To accurately quantify the contents of the collected sample, we followed a procedure described in detail in Ref. [3]. Briefly, we recorded the amount of ^{34}Ar activity retained in the tape as a function of degrader thickness, tracking it from the minimum thickness, at which the ^{34}Ar passed entirely through the tape, to the maximum thickness, which just prevented ^{34}Ar from reaching the tape. This yielded a depth distribution, valid both for ^{34}Ar and for its nearby impurities, and it also produced an experimental measure of the degrader thickness required to stop the main activity midway through the tape. As we have observed in our previous publications, this measured thickness agreed very closely with range calculations by the SRIM code [14], which gives confidence that the code can be relied upon to calculate the ranges of the identified impurities relative to the measured range of ^{34}Ar .

The implantation profiles shown in Fig. 3 apply to the degrader thickness used in our actual measurement. The profiles themselves are derived from the measured ^{34}Ar depth distribution and combine the effects of range straggling and the known momentum spread as set by the momentum-selection slits in MARS ($\Delta p/p = 0.66\%$). The positions of the impurity profiles come from SRIM calculations, and their intensities are set to the values measured at the MARS focal plane (see Fig. 2). The figure makes it clear that the ^{31}S impurity is entirely contained in the tape, while only three-quarters of the ^{32}Cl remains. The third impurity, ^{30}S , passes cleanly through the tape and can thus be eliminated from further consideration. During the collection period, the only impurities implanted in the tape were ^{32}Cl and ^{31}S at rates that were, respectively, 0.08(2)% and 0.13(2)% compared with that of ^{34}Ar . Furthermore, note that ^{32}Cl has a much shorter half-life than ^{34}Ar so its relative contribution to the

activity of the collected sample had decreased significantly by the time the sample reached the detector and counting began. Taking these factors into account, we incorporate both ^{32}Cl and ^{31}S impurities into our analysis.

C. 4π gas counter

Our 4π gas counter consists of two separate gas cells that, when assembled, leave a narrow slot between them, through which the aluminized Mylar transport tape passes. The identical cells each have an active gas volume of about 30 cm^3 , and contain methane at just over 1 atm pressure, which flows slowly through them. As anode, each cell has a single gold-plated tungsten wire $13\text{ }\mu\text{m}$ in diameter. A Havar foil window, 3.7 cm in diameter and $1.5\text{ }\mu\text{m}$ thick, hermetically seals each gas cell on the side facing the tape. The performance of this type of detector is well known [15–17] and the particular detector employed in this measurement is the same one we have used in many previous half-life measurements [9–12]. The detector is nearly 100% efficient for detecting positrons—98.8% by Monte Carlo simulation—while being insensitive to γ radiation.

We characterize the performance of the detector before and after our half-life measurements using a $^{90}\text{Sr}/^{90}\text{Y}$ β source deposited on a piece of transport tape and positioned at the center of the detector where on-line samples stop. We record the count rate from this relatively long-lived source as a function of the applied bias voltage in order to locate the “plateau” region, where the count rate changes by less than 0.5% per 100 V for a range of 200–300 V. This behavior is well understood [15] and establishes the range of bias voltage for which the detector is at full efficiency and has minimal rate dependence. During our ^{34}Ar measurement we operated the gas counter between 2450 and 2650 V, comfortably within the plateau region determined before and after the experiment.

D. Source positioning

To measure a half-life as short as that of ^{34}Ar , the tape transport must operate at high repetition rate. As a mechanical system operating under such demanding conditions, it does not always deliver the implanted source within the normal $\pm 3\text{ mm}$ range around the center of the detector. To identify such cycles, we recorded the number of ions passing through the scintillator on their way to being implanted in the tape, and subsequently the number of positrons detected in the gas counter when that sample reached the counting location. The ratio of detected positrons to implanted heavy ions is sensitive to the positioning of the source, being anomalously low whether the source traveled too far or not far enough. In our final analysis, we accepted those cycles with measured ratios above 94% of the maximum value obtained. We demonstrated this to be a safe limit by performing a separate analysis in which all cycles with a ratio above 91% of the maximum were accepted. The half-life results from the two analyses agreed well within their 0.02% statistical uncertainties.

E. Data acquisition

Data from this measurement were acquired with essentially the same analog electronics we have used in previous

measurements: A detailed description of the setup appears in Ref. [9]. Briefly, signals from the gas counter are fed into a preamplifier followed by a fast timing-filter amplifier set to high gain ($\times 500$). The clipped and amplified signals are then input to a discriminator with a very low threshold (150–250 mV). The discriminator output is split and sent to two fixed-width nonretriggering and nonextending gate generators, which introduce well-known fixed dead times that are selected to be longer than any upstream dead-time contributions. The outputs from the two gate generators are sent to two multi-channel scalers, each with 15 000 channels. The time base for the acquired spectra is defined by a Stanford Research System pulser, which is accurate to 0.01 ppm.

We set the widths of the two gate-generator signals (dead times) to be different from one another and regularly changed them—as well as the detector bias voltage and discriminator level—from run to run as a check on any systematic effects that might arise from these adjustable parameters. We monitored both gates continuously during every run by recording coincidences between each gate and 4-ns-wide pulses from a precise 1-MHz pulse generator; this gave us a continuous measure of the imposed dead times. In this experiment we used dead times of 3, 4, 10, and 12 μs in dead-time channel A, and 4, 6, and 8 μs in channel B.

III. ANALYSIS AND RESULTS

A. Data processing

The first step in data analysis was to reject all faulty cycles. We used two criteria: one to ensure the source was adequately prepared and the other to establish that it was properly delivered to the 4π gas counter. To satisfy the first criterion, we rejected all cycles in which less than one quarter of the normal number of β particles were recorded, an indication of there being very little or no primary beam from the cyclotron during the collection period. This removed $\approx 5\%$ of the cycles.

Our second criterion was based on the ratio of the number of β particles detected to the number of ^{34}Ar ions implanted for each cycle. As explained in Sec. IID we restricted this ratio for a given cycle to between 94% and 100% of the maximum value obtained for the whole run containing that cycle. This removed an additional $\approx 20\%$ of the total cycles.

Data from the remaining 8900 cycles were then corrected cycle by cycle for dead-time losses. The conventional method was used, in which we increased the number of events in each channel of the decay spectrum analytically for the known dominant dead time [17]. Also, as described in Ref. [12], with gas detectors like ours there is a slight increase in detection efficiency with bias voltage even in the “plateau” region where we operate. Because this leads to a very weak dependence of efficiency on counting rate, we used our $^{90}\text{Sr}/^{90}\text{Y}$ β -source measurement of count-rate vs bias (described in Sec. IIC) at our operating voltages to correct our decay data for this effect. Its impact on the ^{34}Ar half-life was small, 0.01%, but not negligible.

For each of our 36 runs we then obtained a decay spectrum by summing the dead-time- and plateau-efficiency-corrected spectra from all the accepted cycles in that run. Finally, with

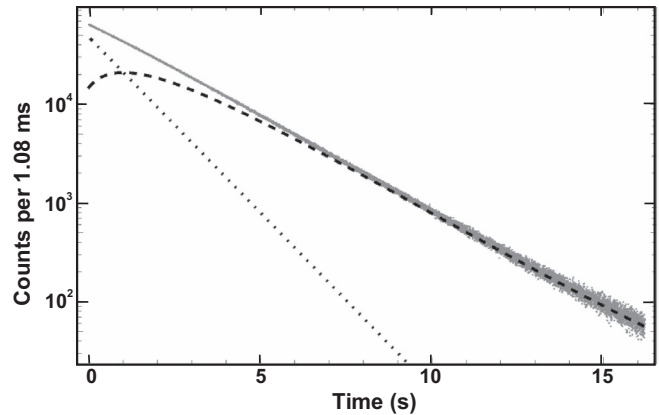


FIG. 4. Measured time-decay spectrum (“solid” band) for the total of all accepted cycles obtained from the decay of ^{34}Ar and its daughter ^{34}Cl . The dotted and dashed lines represent the derived ^{34}Ar and ^{34}Cl contributions, respectively. The constant background is off scale at 9.1 counts/1.08 ms, nearly four orders of magnitude below the initial source counting rate. Note that counting began 210 ms after the beam was turned off, and the measured data are displayed over 15 000 channels.

these spectra in hand we analyzed the runs separately in order to reveal any possible systematic dependence on experimental parameters. This is described in subsequent sections.

However, to demonstrate the quality of the data and the inherent challenge presented by this particular parent-daughter combination, we refer here to Fig. 4, in which all spectra from the individual runs have been summed. Obviously the overall decay curve, which combines the decays of ^{34}Ar and its daughter ^{34}Cl , shows little hint of the parent’s contribution even though it actually dominates at the start of the counting period. Indeed, an uncoupled two-component fit yields a very imprecise result for the ^{34}Ar half-life, even though the ^{34}Cl half-life is well known [1]. What makes it possible for us to extract a useful ^{34}Ar half-life from such spectra is the fact that no ^{34}Cl was deposited in the tape in the first place; it comes exclusively from the decay of ^{34}Ar . By incorporating the parent-daughter coupling into our fitting function, together with fixing the daughter’s precisely known half-life [1], we can achieve good precision in the half-life we obtain for the parent.

B. Parent-daughter connection

The total positron activity from the combined decays of ^{34}Ar and its daughter ^{34}Cl can be described by the coupled decay equations:

$$\Lambda_{\text{total}} = C_1 e^{-\lambda_1 t} + C_2 e^{-\lambda_2 t}, \quad (1)$$

with

$$C_1 = N_1 \epsilon_2 \lambda_1 \left(\frac{\epsilon_1}{\epsilon_2} - \frac{\lambda_2}{\lambda_1 - \lambda_2} \right), \quad (2)$$

$$C_2 = N_1 \epsilon_2 \lambda_2 \left(\frac{N_2}{N_1} + \frac{\lambda_1}{\lambda_1 - \lambda_2} \right),$$

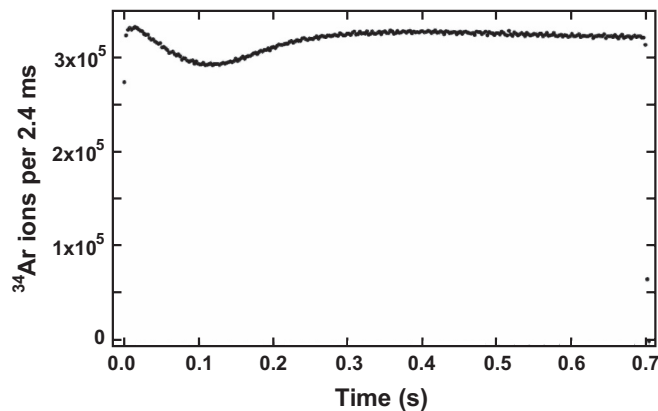


FIG. 5. Measured time profile of the collected ^{34}Ar beam summed for all selected cycles. The initial drop in intensity is generated by the decrease in local density of the hydrogen in the target cell as the primary beam heats the gas around its path. A fan located inside the gas target mitigates the effect and ensures a rapid transition to stable conditions.

where t is the time elapsed after the end of the collection period, $N_{1,2}$ are the numbers of ^{34}Ar and ^{34}Cl nuclei present in the sample at $t = 0$, $\epsilon_{1,2}$ are the efficiencies for detecting the positrons from the respective decays, and $\lambda_{1,2}$ are the corresponding decay constants.

When $\lambda_1/\lambda_2 = 2$ (and $\epsilon_1 = \epsilon_2$) the coefficient C_1 vanishes, leaving a single exponential term having the decay constant of the daughter. For ^{34}Ar and ^{34}Cl , the ratio is 1.8, near enough to the critical value that C_1 is more than a factor of 5 smaller than C_2 . It also is negative, which can be confirmed by a careful examination of Fig. 4.

In fitting the data to extract a half-life, we use the technique we developed in the past, which is based on the maximum-likelihood method. The key element is to fix the ratio of C_2/C_1 so that the number of adjustable parameters in the fit is reduced to three, including background. We have already used this approach to measure the half-lives of other parent-daughter pairs: $^{26}\text{Si}/^{26m}\text{Al}$ [10], $^{38}\text{Ca}/^{38m}\text{K}$ [11], and $^{30}\text{S}/^{30}\text{P}$ [12]. In the third case, the half-lives of the parent and daughter are very different from one another so we could determine the parent's half-life in two ways, either by treating the pair as a coupled parent and daughter or as two independent decays. The two results we obtained agreed well with one another [12], thus confirming the efficacy of the coupled approach, which in our present case is the only viable option.

To establish the value of C_2/C_1 we must first determine two other ratios, N_2/N_1 and ϵ_1/ϵ_2 . The first would be simple to calculate from the production of ^{34}Cl (via ^{34}Ar decay) over the collection period if the collection rate for ^{34}Ar were exactly constant over that period. However, for the precision we seek, it is not enough to assume approximate constancy. Instead we recorded the number of ^{34}Ar ions passing through the scintillator at the exit of MARS as a function of time for each cycle. A typical result, summed over the cycles in one run, is shown in Fig. 5. It can be seen that there is some variation in the collection rate, particularly over the

first half of each collection period, caused by local heating and a concomitant drop in gas density along the path of the primary beam inside the gas cell, before an internal fan restores equilibrium.

By using this measured ^{34}Ar collection rate, we could obtain the decay production of ^{34}Cl from a numerical integration over the whole collection period, and hence determine N_2/N_1 for each run. This calculation of course depends on λ_1 (and λ_2) so, in practice, when we fitted our decay data, the integration was incorporated into our fitting function, with λ_1 being common to the ratio determination and the calculated decay curve.

C. Parent-daughter efficiency ratios, ϵ_1/ϵ_2

Because the decay positrons from both ^{34}Ar and its daughter were detected in the same detector with identical geometry and a very low electronic threshold (see Sec. II E), their detection efficiencies are very nearly the same. What causes them to differ slightly is an energy threshold unassociated with the electronic one, which arises from the fact that low-energy positrons are stopped in the aluminized Mylar transport tape (with half-thickness of $38\ \mu\text{m}$) and in the Havar windows of the gas counter ($1.5\ \mu\text{m}$ thick), consequently never reaching the active volume of the detector. The β end-point energy for ^{34}Ar is 5040 keV, while that for ^{34}Cl is 4470 keV, so the energy threshold, which is the same for both, cuts out a smaller fraction of the ^{34}Ar decays than it does for the ^{34}Cl decays. The efficiency for detecting the ^{34}Cl positrons is thus slightly less than for detecting the ^{34}Ar positrons.

To express this efficiency difference quantitatively, we follow the procedure we have used—and described in detail—in earlier measurements of the half-lives of ^{26}Si [10] and ^{38}Ca [11]. We first calculated the total positron-decay spectra for both parent and daughter, including the relatively weak Gamow-Teller branches in the ^{34}Ar decay spectrum. Then we evaluated the effective energy threshold by modeling our exact tape-window-detector geometry within the Monte Carlo code EGSNRC (release 2018) [18]; because the decay positrons are emitted isotropically, their paths through the tape and window span a range of lengths, resulting in a low-energy cutoff that is not sharp. Finally, we convolved the Monte Carlo result with each positron spectrum to obtain the detection efficiency for each decay. The result showed the efficiency for detecting ^{34}Ar positrons was 0.026(22)% greater than the efficiency for detecting positrons from ^{34}Cl , where the uncertainty arises from the statistical uncertainty of the Monte Carlo calculation and from our assigning a $\pm 10\%$ relative uncertainty on the calculated ranges.

There is one additional factor that contributes to the parent-daughter efficiency ratio: A very weak decay path from ^{34}Ar does not ultimately feed the short-lived ground state of ^{34}Cl but instead populates the 32-min isomeric state at 146 keV, whose decay would be unobserved during our 16.2-s counting period. This “leakage” from the strict parent-daughter connection occurs via the 519-keV γ ray, which deexcites the 666-keV state in weak competition with the predominant γ ray to the ground state. A recent measurement specifically focused on the decay of the 666-keV level has established

that the intensity of the 519-keV γ ray is 1.46(19)% that of the 666-keV γ ray [7]. This represents a 0.036(5)% leakage from the decay paths that feed the ^{34}Cl ground state, and can simply be treated as a further small reduction in the detection efficiency for the ^{34}Cl decay.

Incorporating both these effects into the efficiency ratio, we obtain $\epsilon_1/\epsilon_2 = 1.00062(23)$.

D. Half-life determination

The dead-time- and plateau-efficiency-corrected data from each of the 36 runs (see Sec. III A) were fitted separately. We used maximum likelihood for Poisson distributed data, and incorporated five components: ^{34}Ar , its daughter ^{34}Cl , the impurities ^{32}Cl and ^{31}S , and a constant background. The half-life of ^{34}Cl was fixed at its world-average value of 1526.55(44) ms [1], and the ratio of its initial detected activity relative to that of ^{34}Ar was obtained for each run from numerical integration of the measured ^{34}Ar beam profile as a function of time in that run (see Sec. III B and Fig. 5), combined with the efficiency ratio ϵ_1/ϵ_2 derived in Sec. III C. The half-lives of ^{32}Cl and ^{31}S were fixed at 298(1) ms [19] and 2.5534(18) s [20], respectively; with their relative intensities taken from the measurements and calculations described in Sec. II B.

During our experiment, we measured the β -detector background rate by disabling the tape motion in one run while maintaining all the other conditions as they were in a normal run. As a further check, in preliminary fits of the ^{34}Ar decay data we also left the background rate as a parameter to be fitted. We found very little scatter in the fitted background rates from run to run, and the average value for all runs agreed well with the result from the dedicated background run. Thus, in the final analysis we fixed the background rate at 0.96(6) counts/s, leaving N_1 and the ^{34}Ar half-life as the two parameters to be determined. In each decay spectrum, the background rate was about four orders of magnitude below the initial source decay rate, so its quoted uncertainty has a relatively small impact on the half-life result.

With our gas detector operating in the plateau region and using the same equipment as employed here, we have demonstrated in the past (e.g., [10–12,21]) that our half-life results are independent of the values chosen for the three measurement parameters: detector bias, discriminator threshold setting, and dominant dead time. Nevertheless, we tested here again for any hints of systematic dependence on those settings. Panels (a)–(c) of Fig. 6 each include half-life results from all 36 runs, but the runs are grouped differently in each panel, according to the parameter being investigated. It can be clearly seen that there is no statistically significant dependence on any of the three detection settings. The figure illustrates the results from dead-time channel A, but the behavior of channel B is entirely equivalent.

Having eliminated any significant dependence of our results on the measurement parameters, we can now obtain the final average value for the half-life of ^{34}Ar , taking account of results from both dead-time channels. The result is $t_{1/2}(^{34}\text{Ar}) = 0.84646(19)$ s, where the quoted uncertainty is purely statistical and has already been multiplied by the square

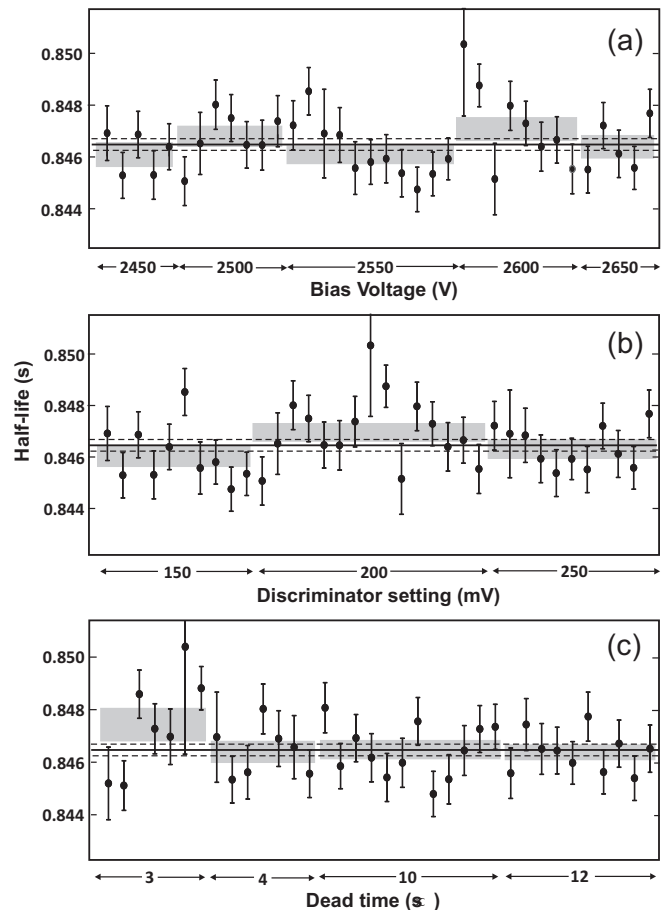


FIG. 6. Test for systematic bias in the ^{34}Ar half-life results as a function of (a) detector voltage, (b) discriminator setting, and (c) imposed dead time. All 36 runs are included in each plot, but they have been grouped differently to focus on a particular detection parameter. In all cases, grey bands represent the $\pm\sigma$ limits of the average half-life for a given condition. The average value for all the runs appears as a solid horizontal line in each plot, with the corresponding dashed lines showing the statistical uncertainty limits. The value of the reduced χ^2 for the 36-point average is 1.34. The results from dead-time channel A are shown; channel B results are equivalently satisfactory.

root of 1.34, the reduced χ^2 . This average appears in each panel of Fig. 6 as a solid line with dashed lines on either side to represent uncertainty limits.

We can now perform one final test, which would be sensitive to the presence of unanticipated short-lived impurities or of electronic counting-rate-dependent effects, if they existed. Having already obtained an average half-life from the full set of data, we proceeded to eliminate data from the first 195 ms of the counting period for each cycle and fit the remaining data again to obtain an average half-life; then we removed another 195 ms and fitted again. This procedure was repeated until data from 2.124 s (2.5 half-lives of ^{34}Ar) had been eliminated. The results for dead-time channel A are illustrated in Fig. 7, where they show no evidence of any systematic effects. Channel B is not shown but it is equally convincing. This demonstrated rate independence is consistent with an

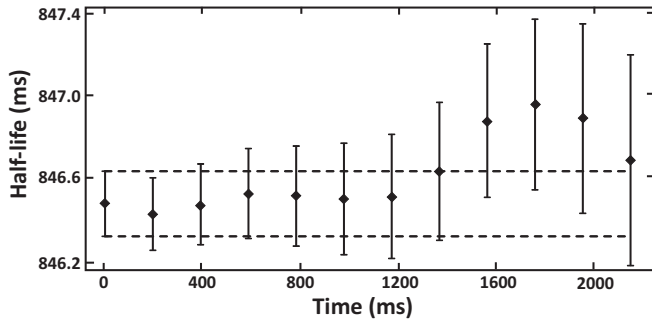


FIG. 7. Test for systematic bias in the ^{34}Ar half-life results due to otherwise undetected short-lived impurities or rate-dependent effects. Each point results from a separate fit to the data from dead-time channel A; the abscissa for each point represents the time period at the beginning of the counting cycle for which the data were omitted from that particular fit. The dashed lines correspond to the $\pm\sigma$ uncertainty limits for the full data set.

independent test we reported recently [12], in which we proved that, at the current level of precision, our system shows no signs of rate-dependent effects up to an initial count rate of at least 9×10^3 counts/s and probably well above that. The highest initial count rate recorded in the present measurement was 9.4×10^3 counts/s.

So far the only uncertainty we have quoted for the ^{34}Ar half-life is due to counting statistics. We have also demonstrated that any contributions from systematic instrumental effects must be well below our statistical sensitivity and consequently cannot be precisely quantified. Whatever small effects there might be, though, have surely been subsumed into the scale factor—the square root of the reduced χ^2 —which has already been included in the statistical uncertainty on our average half-life. It only remains then for us to take account of uncertainties in the half-life of ^{34}Cl , the efficiency ratio for detecting parent and daughter activities, the background counting rate, and the intensity of the impurities collected in each sample, all of which were input parameters in our fitting procedure. The overall uncertainty budget is presented in Table I.

The fact that the uncertainty in the half-life of ^{34}Cl , which is a mere $\pm 0.03\%$, is the largest contributor to our overall uncertainty is a reflection of the unbreakable connection between the parent and daughter decays that is inherent to our measurement technique. The second largest contribution

TABLE I. Uncertainty budget for our ^{34}Ar half-life measurement.

Source	Uncertainty (ms)
statistics	0.19
^{34}Cl half-life	0.23
background	0.15
efficiency ratio, ϵ_1/ϵ_2	0.09
sample impurities (^{32}Cl , ^{31}S)	0.06
Total	0.35
^{34}Ar half-life result	0.84646(35) s

comes from counting statistics, with the background rate and efficiency ratio being the next most significant. Lastly, in this particular measurement, the sample impurities were small enough that they had very little impact on the half-life uncertainty. We remark that the uncertainty attributed to the background could have been reduced had we counted each sample long enough for the decay curve to have reached the level of background (see Fig. 4) but this would have reduced the overall counting efficiency for our allotted accelerator time. The loss in counting statistics would have increased our uncertainty more than the gain in background precision would have reduced it. Our final result for the half-life of ^{34}Ar is 0.84646(35) s, in which statistical and systematic uncertainties have been combined.

E. Comparison with previous measurements

There have been four previous measurements of the ^{34}Ar half-life [5], but only two of them produced a result with sufficient precision to be listed as relevant in the most recent survey of superallowed $0^+ \rightarrow 0^+$ β decay [1]: 0.8445(34) s [8] and 0.8438(4) s [9]. The first, and least precise, of these previous results agrees well with our new half-life, but the second has only a slightly larger uncertainty than the one we quote here, yet it differs from our result by nearly seven times that uncertainty. Regrettably, that discrepant measurement is also ours, made 13 years ago with an early version of the equipment and some of the analysis methods used in the present measurement.

That earlier measurement was our first to extract the parent half-life from a mixed parent-daughter pair of superallowed emitters. From subsequent tests and experience, we recognized that there had been some notable omissions in the first experiment and its analysis. This prompted us over a decade ago to implement significant improvements before making more measurements of the same type [10–12]. Only recently, though, did we realize that the omissions could have had a serious impact on our published ^{34}Ar half-life result [9]. This motivated our new measurement. The most important improvements that distinguish it from the old one are as follows:

- (i) In Ref. [9] we recorded the ^{34}Ar beam and impurities at the focal plane of MARS only once, immediately before the measurement began. We soon learned that more frequent checks are necessary, with occasional minor retuning of MARS. Also, the impurities were much more intense than in the measurement reported here. Impurities are now under much better control (see Sec. II B).
- (ii) In Ref. [9] we recorded the time profile of the collected ^{34}Ar beam in a separate experiment. In subsequent measurements, we have recorded it for each cycle (see Sec. III B), thus accounting for any dependence on beam current.
- (iii) In applying Eq. (2) in Ref. [9], we used $\epsilon_1/\epsilon_2 = 1$. We had not recognized the subtle difference in β -detection efficiency between parent and daughter decays. Also the weak γ -decay branch from the

666-keV state to the 146-keV isomeric state in ^{34}Cl , which introduces “leakage” into the parent-daughter connection, was unknown and unsuspected at that time. We now take account of both effects (see Sec. III C).

In addition to correcting these critical omissions, our new measurement incorporates many other improvements to our data acquisition and analysis. For example, in Ref. [9] we recorded 500-channel time-decay spectra and analyzed them using a procedure to minimize χ^2 (Gauss style) with weights and variances optimized for dead-time-distorted Poisson data [17]. Now we record 15 000-channel spectra and use consistent Poisson statistics and the maximum-likelihood criterion throughout the analysis (see Sec. III D).

In light of the omissions in Ref. [9], which we have itemized here, we consider it appropriate to withdraw the ^{34}Ar half-life we published there [9], and replace it with the value we have obtained in this new measurement.

IV. CONCLUSIONS

We report here a new half-life for ^{34}Ar of 0.84646(35) s, which has a precision of $\pm 0.04\%$. Because ^{34}Ar and its daughter ^{34}Cl are both positron emitters with comparable half-lives, we used a technique in which the parent and daughter decays can be linked by means of a precise measurement of the deposition rate for a nearly pure sample. This is a technique we have been refining for more than a decade [9–12]. For reasons we have enunciated here, we conclude that the result we obtained for ^{34}Ar in our first measurement of this type in 2006 [9] suffered from several important omissions that were corrected in subsequent measurements. Herewith,

we withdraw that 2006 result and replace it with a new half-life value.

We can now obtain the ft value for the superallowed $0^+ \rightarrow 0^+$ β transition in the decay of ^{34}Ar by combining our new half-life result with the corresponding Q_{EC} value and branching ratio taken from the most recent survey of world data [1]. When the result, $ft = 3059(8)$ s, is corrected for the radiative and isospin-symmetry-breaking effects also tabulated in Ref. [1], we obtain a corrected $\mathcal{F}t$ value for the ^{34}Ar superallowed transition of 3075(8) s. This is nearly 10 s higher than the previously accepted value and is much closer to the average value for the 14 well-measured transitions: $\overline{\mathcal{F}t} = 3072.27(62)$ s.

We note that the uncertainty on the ^{34}Ar $\mathcal{F}t$ value is dominated by the branching-ratio uncertainty for the superallowed transition. We are now well advanced on a new measurement of that branching ratio, with a view to being able to considerably reduce its uncertainty, and consequently improve the ^{34}Ar ft - and $\mathcal{F}t$ -value uncertainties as well. Most importantly, this would complete another mirror pair of superallowed $0^+ \rightarrow 0^+$ β transitions, $^{34}\text{Ar} \rightarrow ^{34}\text{Cl}$ and $^{34}\text{Cl} \rightarrow ^{34}\text{S}$, which would contribute to a critical test of the isospin-symmetry-breaking corrections used to obtain $\mathcal{F}t$ and, ultimately, V_{ud} [4].

ACKNOWLEDGMENTS

This material is based upon work supported by the US Department of Energy, Office of Science, Office of Nuclear Physics, under Grant No. DE-FG03-93ER40773, and by the Welch Foundation under Grant No. A-1397.

-
- [1] J. C. Hardy and I. S. Towner, *Phys. Rev. C* **91**, 025501 (2015).
 [2] H. I. Park, J. C. Hardy, V. E. Iacob, M. Bencomo, L. Chen, V. Horvat, N. Nica, B. T. Roeder, E. McCleskey, R. E. Tribble, and I. S. Towner, *Phys. Rev. C* **92**, 015502 (2015).
 [3] M. Bencomo, J. C. Hardy, V. E. Iacob, H. I. Park, L. Chen, V. Horvat, N. Nica, B. T. Roeder, A. Saastamoinen, and I. S. Towner, *Phys. Rev. C* **100**, 015503 (2019).
 [4] H. I. Park, J. C. Hardy, V. E. Iacob, M. Bencomo, L. Chen, V. Horvat, N. Nica, B. T. Roeder, E. Simmons, R. E. Tribble, and I. S. Towner, *Phys. Rev. Lett.* **112**, 102502 (2014).
 [5] N. Nica and B. Singh, *Nucl. Data Sheets* **113**, 1563 (2012).
 [6] V. E. Iacob, J. C. Hardy, H. I. Park, M. Bencomo, L. Chen, V. Horvat, N. Nica, B. T. Roeder, A. Saastamoinen, and I. S. Towner (unpublished).
 [7] H. I. Park *et al.* (unpublished).
 [8] J. C. Hardy, H. Schmeing, J. S. Geiger, and R. L. Graham, *Nucl. Phys. A* **223**, 157 (1974).
 [9] V. E. Iacob, J. C. Hardy, J. F. Brinkley, C. A. Gagliardi, V. E. Mayes, N. Nica, M. Sanchez-Vega, G. Tabacaru, L. Trache, and R. E. Tribble, *Phys. Rev. C* **74**, 055502 (2006).
 [10] V. E. Iacob, J. C. Hardy, A. Banu, L. Chen, V. V. Golovko, J. Goodwin, V. Horvat, N. Nica, H. I. Park, L. Trache, and R. E. Tribble, *Phys. Rev. C* **82**, 035502 (2010).
 [11] H. I. Park, J. C. Hardy, V. E. Iacob, A. Banu, L. Chen, V. V. Golovko, J. Goodwin, V. Horvat, N. Nica, E. Simmons, L. Trache, and R. E. Tribble, *Phys. Rev. C* **84**, 065502 (2011).
 [12] V. E. Iacob, J. C. Hardy, L. Chen, V. Horvat, M. Bencomo, N. Nica, H. I. Park, B. T. Roeder, and A. Saastamoinen, *Phys. Rev. C* **97**, 035501 (2018).
 [13] R. E. Tribble, A. Azhari, C. A. Gagliardi, J. C. Hardy, A. Mukhamedzhanov, X. Tang, L. Trache, and S. J. Yennello, *Nucl. Phys. A* **701**, 278 (2002).
 [14] J. F. Ziegler, <http://www.srim.org/>.
 [15] *A Handbook of Radioactivity Measurements Procedures*, National Council on Radiation Protection and Measurements Report NCRP No. 58, 1978 (unpublished), see especially Sec. 3.5.
 [16] V. T. Koslowsky, E. Hagberg, J. C. Hardy, R. E. Azuma, E. T. H. Clifford, H. C. Evans, H. Schmeing, U. J. Schrewe, and K. S. Sharma, *Nucl. Phys. A* **405**, 29 (1983).
 [17] V. T. Koslowsky, E. Hagberg, J. C. Hardy, G. Savard, H. Schmeing, K. S. Sharma, and X. J. Sun, *Nucl. Instrum. Methods Phys. Res. A* **401**, 289 (1997).
 [18] I. Kawrakow, *Med. Phys.* **27**, 485 (2000); I. Kawrakow and D. W. O. Rogers, National Research Council Canada Report No. PIRS-701, NRC, Ottawa, 2003 (unpublished), <http://nrc-cnrc.github.io/EGSnrc/>.
 [19] C. Ouellet and B. Singh, *Nucl. Data Sheets* **112**, 2199 (2011).
 [20] C. Ouellet and B. Singh, *Nucl. Data Sheets* **114**, 209 (2013).
 [21] H. I. Park, J. C. Hardy, V. E. Iacob, L. Chen, J. Goodwin, N. Nica, E. Simmons, L. Trache, and R. E. Tribble, *Phys. Rev. C* **85**, 035501 (2012).